EUMETSAT OSI SAF
OCEAN AND SEA ICE

# The EUMETSAT OSI SAF Level-2 Sea-Ice Concentration Algorithm

Product OSI-410

Version : 1.3

Date : 07/07/2020

John Lavelle and Rasmus Tonboe

Danmarks Meteorologiske Institut

# Document Change record

| Document version | Software version | Date | Author | Change description |
|---|---|---|---|---|
| V 1.0 - draft | V 1.0 | 06-03-2019 | John Lavelle | First version ready for PCR review |
| V 1.1 | V1.0 | 03-06-19 | John Lavelle | Updated after PCR review according to RIDs |
| V1.2 | | 15-01-20 | John Lavelle | Updated with sections on climatology mask and land/lake mask.<br>Prepared for ORR review. |
| V1.3 | V1.0 | 07-07-20 | Rasmus Tonboe | Update after ORR |

# Table of Contents

# 1. Introduction

The EUMETSAT Ocean and Sea Ice SAF

The Satellite Application Facilities (SAFs) are dedicated centres of excellence for processing satellite data – hosted by a National Meteorological Service – which utilise specialist expertise from institutes based in Member States. EUMETSAT created Satellite Application Facilities (SAFs) to complement its Central Facilities capability in Darmstadt. The Ocean and Sea Ice Satellite Application Facility (OSI SAF) is one of eight EUMETSAT SAFs, which provide users with operational data and software products. More on SAFs can be read at www.eumetsat.int.

The objective of the OSI SAF is the operational near real-time production and distribution of a coherent set of information, derived from earth observation satellites, and characterising the ocean surface and the energy fluxes through it: sea surface temperature, radiative fluxes, wind vector and sea ice characteristics. For some variables, the OSI SAF is also aiming at providing long term data records for climate applications, based on reprocessing activities.

The OSI SAF consortium is hosted by Météo-France. The sea ice processing is performed at the High Latitude processing facility (HL centre), operated jointly by the Norwegian and Danish Meteorological Institutes. The sea ice products include sea ice concentration, the sea ice emissivity at 50 GHz, sea ice edge, sea ice type and sea ice drift and sea ice surface temperature (from mid 2014).

## 1.1. Disclaimer



Note : The comments that we get from our users is an important input when defining development activities and updates, and user feedback to the OSI SAF project team is highly valued.

**Acknowledgement and citation**

Use of the product(s) should be acknowledged with the following citations (product specific):
OSI-410 : OSI SAF (2020): Global Sea Ice Concentration Level 2, EUMETSAT SAF on Ocean and Sea Ice.

## 1.2. Scope of this document

This document describes OSI-410, the Level 2 global sea-ice concentration product. The product is derived from passive microwave measurements from the SSMIS and AMSR-2 instruments on-board the DMSP and JAXA's GCOM-W1 polar orbiting satellites respectively.

This *Level 2* product is derived from *Level 1* passive microwave satellite products, with one file for each corresponding Level 1 swath file. Each OSI-410 product file is calculated from either an AMSR-2 or SSMIS, Level 1, swath. The processing steps are similar for each of the instruments; however, as described in Sections 3 and 6, as channel frequencies and footprints of the instruments are not identical, there are some differences.

The two level 3 products OSI-401-b and OSI-408, are daily gridded sea-ice concentration products, covering the Northern and Southern Hemispheres. The Level 2 product is for users who require a temporal resolution of better than 24 hours and/or reduced timeliness compared to the Level 3 product.

The level 3 sea ice concentration product is available 6 hours after midnight on the following days morning. Data used in the level 3 product are collected for a full day from 00 to 24 hours. The requirements to the level 2 product timeliness is that the products should be available to the user 220 minutes after satellite overpass (3 hours and 40 minutes). In practise it is expected that the products can be available to the user much faster than that.

In addition to the timeliness of the L2 product compared to L3 the L2 product has also lower uncertainty. This is because the L2 sea-ice concentration products are not re-sampled and the original satellite projection is retained. This lower uncertainty is only achieved when the data are used together with a footprint operator so that the extent and weighting of the measurement is included.

## 1.3. Glossary

| | |
|---|---|
| AMSR-2 | Advanced Microwave Scanning Radiometer 2 |
| ATBD | Algorithm Theoretical Basis Doccument |
| CDOP | Continuous Development and Operations Phase (OSI SAF project) |
| CMS | Centre de Météorologie Spatiale |
| DMI | Danish Meteorological Institute |
| DMSP | Defense Meteorological Satellite Program |
| ECMWF | European Centre for Medium range Weather Forecast |
| ESA SICCI | European Space Agency Sea Ice Climate Change Initiative |
| EUMETSAT | European Organization for the Exploitation of Meteorological Satellites |
| FWHM | Full Width at Half Maximum |
| met.no | Norwegian Meteorological Institute |
| NASA | National Aeronautics and Space Administration |
| NSIDC | National Snow and Ice Data Center |
| NT | NASA Team |
| NWP | Numerical Weather Prediction |
| OSI SAF | Ocean and Sea Ice Satellite Application Facility |
| RTM | Radiative Transfer Model |
| SAR | Synthetic Aperture Radar |
| SICCI | Sea Ice Climate Change Initiative |
| SMMR | Scanning Multi-channel Microwave Radiometer |
| SSM/I | Special Sensor Microwave/Imager |
| SSMIS | Special Sensor Microwave Imager / Sounder |
| SST | Sea surface temperature |
| TUD | Technical University of Denmark |

## 1.4. Reference and applicable Documents

### *1.4.1. Reference documents*

[RD.1] OSI SAF Global sea-ice Concentration Reprocessing Product User Manual (OSI-401-b), version 1.6. Available at http://osisaf.met.no/docs.

[RD.2] ATBD for OSI SAF Global Reprocessed sea-ice Concentration Product (OSI-409, OSI-409a, OSI-430), version 1.1. Available at http://osisaf.met.no/docs.

[RD.3] Algorithm Theoretical Basis Document for the AMSR-2 sea-ice Concentration product (OSI-408), version 1.0. Available at http://osisaf.met.no/docs.

### *1.4.2. Applicable documents*

[AD.1] EUMETSAT OSI SAF *Product Requirements Document.* SAF/OSI/CDOP3/MF/MGT/PL/2-001, version 1.4, 20/12/2018

# 2. Processing chain overview

Each of the sea-ice concentration algorithms are based on the principle that it is possible to distinguish sea-ice and water with a passive microwave instrument, due to the difference in their emissivity signatures. The OSI-410 products are generated out of approximately 15 SSMIS swaths per day and 29 AMSR2 swaths per day together with NWP data from ECMWF. The input data, in the case of SSMIS it is received from EUMETSAT via EUMETCast, in the case of AMSR2 it is downloaded directly from JAXA. There are three separate Level 2 products: one for each SSMIS swath (computed using the OSI Hybrid algorithm (see Section 6.1)) and two for each AMSR-2 swath (one computed using the OSI Hybrid algorithm and the other, higher resolution product, computed with the TUD algorithm (see Section 6)). The steps in the processing chain of the Level 2 sea-ice concentration products are shown in Figure 1; these steps are essentially the same for each of the three products. The passive microwave brightness temperatures (Level 1 product) described in Section 3, are the input to the processing chain. Firstly, as described in Section 4, the Radiative Transfer Model (RTM) is applied to estimate the surface level brightness temperatures at sea-level, from the top of the atmosphere measurements. In the next step (as described in Section 5) the dynamic tie points are computed, these are used in the ice concentration algorithm to reduce the sensitivity to inter-annual and climatic variability in the sea-ice and water signatures, and sensor drift. The sea-ice concentration algorithm is described in Section 6. The sea-ice concentration is given at the same coordinates of the swaths. Climatology masks and land/lake mask are then applied to the product, as described in Sections 8 and 9 respectively. The uncertainties for each sea-ice concentration are also included in the product; they are computed as described in Section 7.

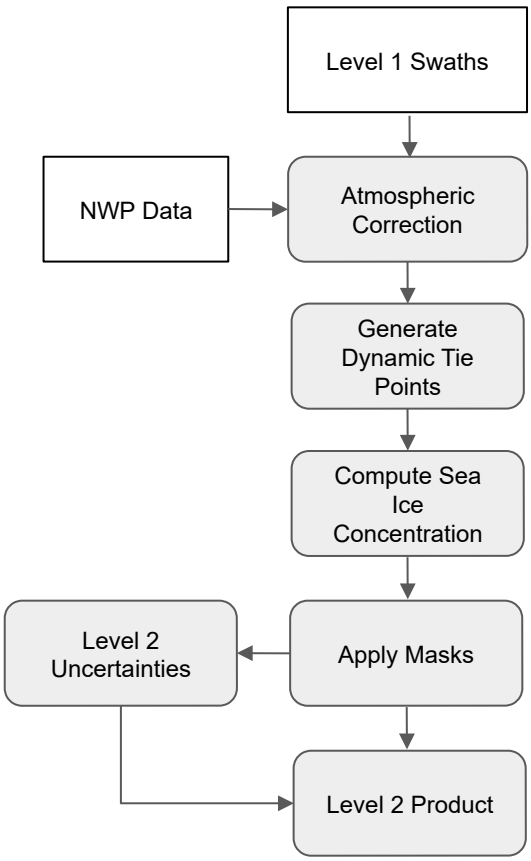

Figure 1: Flow chart for the OSI 410 Level 2 production chain.

# 3. Level 1 data

The Level 2 product is computed from SSMIS and AMSR-2 Level 1 data. SSMIS and AMSR-2 instruments are polar orbiting conically scanning radiometers. The AMSR-2 had a larger antenna, giving it a higher spatial resolution.

## 3.1. SSMIS

SSMIS is the successor to the Special Sensor Microwave/Imager (SSM/I). SSMIS is flown on board the United States Air Force (DMSP) series of satellites, F-16, F-17, F-18 and F-19, which came into operation on November 2005, March 2008 March 2016 and May 2016, respectively (however, F-19 has not been operational since February 2016). The SSMIS instrument has a 0.8 m diameter antenna, a constant incidence angle 53.1° and a swath width of about 1700 km. The instrument has 24 channels from 19 to 183 GHz; the sea-ice concentration algorithm uses the channels given in Table 1.

| Centre freq. (nominal) (GHz) | Polarization | Bandwidth (MHz) | Footprint (km x km) | Sampling Interval (km) |
|---|---|---|---|---|
| 19.35 (19) | V | 356 | 42.4 × 70.1 | 12.5 |
| 37 (37) | H & V | 1.580 | 27.5 × 44.2 | |

*Table 1: SSMIS channels used in the sea-ice concentration algorithms.*

### 3.2. AMSR-2

AMSR-2 is the successor to ADEOS-II and AMSR for EOS (AMSR-E). The AMSR-2 instrument was launched in May 2012. The instrument a 2 m diameter antenna, a constant incidence angle of 55° and a swath width of 1450 km. The instrument has channels covering from 6.925 GHz to 89.0 GHz, with both horizontal and vertical polarizations. The sea-ice concentration algorithms use the channels given in Table 2.

| Centre freq. (nominal) (GHz) | Polarization | Bandwidth (MHz) | Footprint (km x km) | Sampling Interval (km) |
|---|---|---|---|---|
| 18.70 (19) | V | 200 | 14 × 22 | 10 |
| 36.50 (37) | H & V | 1.000 | 7 × 12 | |
| 89.00 (89) | V | 3.000 | 3 × 5 | 5 |

*Table 2: AMSR-2 channels used in the sea-ice concentration algorithms. The footprint size is the instantaneous footprint size.*

## 4. Radiative Transfer Model

The atmospheric water content and wind roughening of the open sea surface can sometimes be problematic for sea-ice concentration retrievals. The brightness temperatures ($T_b$s) are explicitly corrected for wind roughening over open water and water vapour in the atmosphere, prior to the calculation of sea-ice concentration. The correction uses both RTM and NWP data. Over areas with both sea-ice and water, the influence of open water roughness on the $T_b$s and the sea-ice emissivity scales linearly with the sea-ice concentration. The emissivity of sea-ice is determined from standard tie-point emissivities. The correction procedure is described in detail in Andersen et al. (2006B). For a given satellite swath, the closest in time NWP output is found and the NWP model grid points are spatially resampled to the satellite swath grid., then the $T_b$ s are corrected with this matched NWP data.

The following prognostic variables are taken from the ECMWF operational forecast model output: 10 m wind speed ($W$), 2 m air temperature ($T_s$), total column water vapour ($V$), total column cloud liquid water ($L$).

Parameters such as $T_s$, $W$ and $V$ are well represented by the NWP models (at least in the short-term forecasts). However, the representation of cloud liquid water column in the NWP data is not suitable for use for $T_b$ correction (see Andersen et al., 2006B). The $T_b$s are therefore *not* corrected for the influence

of cloud liquid water following the procedure in Andersen et al. (2006B) and in Ivanova et al. (2015) and $L$ is set to zero in the RTM. The RTM described in Wentz (1997) and adopted by Wentz and Meissner (2000), is used for the AMSR-2 processing. Based on these two references, the model is briefly described in the following section.

Using the model function presented in this section, the $T_b$s are corrected for the influence of water vapour in the atmosphere and open water surface roughness caused by wind shear. The model function is a semi-empirical radiative transfer ocean model, describing $T_b$ as a function of sea surface temperature, surface wind friction velocity, total atmospheric water vapour, total cloud liquid water and surface air temperature. The model function was used for SSMI processing and described in Wentz (1997), and has been adopted by Wentz and Meissner (2000) for AMSR processing, with consideration of differences in frequencies, polarization and incidence angle from previous satellite radiometers.

The correction procedure is described in Andersen et al. (2006B). At intermediate sea-ice concentrations the surface emission term is a linear combination of sea-ice emissivity derived from tie-point signatures and the open water emissivity derived from the model.

The model function employs the simplified radiative transfer function for isotropic conditions (which is adequate for many applications, including this one) together with regressions describing the sensitivity to atmospheric and surface parameters. The radiative transfer equation for the top of the atmosphere brightness temperature, $F$, is given by

$$F(W,V,L)=T_{BU}+\tau[ET_S+(1-E)(\Omega T_{BD}+\tau T_C)], \quad (1)$$

where $V$ (mm) is the vertically integrated water vapour, $W$ (m/s) is the wind speed (at 10 m) and $L$ (mm) is the vertically integrated cloud liquid water (here $L = 0$). $T_{BU}$ and $T_{BD}$ are the upwelling and down-welling atmospheric brightness temperatures and $\tau$ is the atmospheric transmittance. $E$ is the sea surface emissivity and $T_S$ is the sea surface temperature. $T_C$ is the cosmic background radiation temperature, equalling 2.7 K. All temperatures are in Kelvins. The $\Omega$ term is the reflection reduction factor due to wind induced sea surface roughness.

The upwelling and down-welling brightness temperatures are expressed in terms of effective air temperatures, $T_U$ and $T_D$, defined by

$$T_U=\frac{T_{BU}}{(1-\tau)} \quad (2a)$$

$$T_D=\frac{T_{BD}}{(1-\tau)}. \quad (2b)$$

$T_U$ is a few degrees colder than $T_D$. In Wentz (1997), using a radiosonde dataset from sites located around the Global Ocean, it was found that $T_U$ and $T_D$ were highly correlated with $V$ and $T_S$.. The following least squares regressions are given as (see Equations 26-27 in Wentz and Meissner, 2000):

$$T_D=b_0+b_1V+b_2V^2+b_3V^3+b_4V^4+b_5\varsigma(T_S-T_V) \quad (3a)$$

$$T_U=T_D+b_6+b_7V, \quad (3b)$$

where

$$T_V = 273.16 + 0.8337V - 3.029\,10^{-5}V^{3.33} \qquad V \leq 48 \qquad (4a)$$

$$T_V = 301.16 \qquad V > 48 \qquad (4b)$$

and

$$\varsigma(T_S - T_V) = 1.05(T_S - T_V)[1 - (T_S - T_V)^2/1200] \qquad |T_S - T_V| \leq 20K \qquad (4c)$$

$$\varsigma(T_S - T_V) = sign(T_S - T_V)14\,K \qquad |T_S - T_V| > 20K. \qquad (4d)$$

The regression coefficients $b$ in Eqs. 3 are given in Table 3. Equations 4a and 4b are found by regressing the $T_S$ climatology at the radiosonde site to $V$. Thus, $T_V$ represents sea surface temperature for given water vapour in the atmosphere. Wentz and Meissner (2000) include a function of the difference between the sea surface temperature $T_S$ and $T_V$. The term $\varsigma(T_S\text{-}T_V)$ accounts for the fact that the effective air temperature is typically higher (or lower) for the case of unusually warm (or cold) water. Here, scattering by cloud liquid water is neglected

| Coeff.\Freq. | 19 GHz | 37 GHz | 89 GHz |
|---|---|---|---|
| $b_0$ (K) | 2.402E+02 | 2.395E+02 | 2.426E+02 |
| $b_1$ (K mm$^{-1}$) | 2.989E+00 | 2.544E+00 | 3.023E+00 |
| $b_2$ (K mm$^{-2}$) | -7.259E-02 | -5.128E-02 | -7.498E-02 |
| $b_3$ (K mm$^{-3}$) | 8.145E-04 | 4.520E-04 | 8.807E-04 |
| $b_4$ (K mm$^{-4}$) | -3.607E-06 | -1.436E-06 | -4.088E-06 |
| $b_5$ | 6.100E-01 | 5.800E-01 | 6.200E-01 |
| $b_6$ (K) | -1.600E-01 | -5.700E-01 | -5.700E-01 |
| $b_7$ (K mm$^{-1}$) | -1.690E-02 | -2.380E-02 | -8.070E-02 |
| $a_{O1}$ | 1.215E-02 | 4.006E-02 | 5.335E-02 |
| $a_{O2}$ (K) | -6.100E-05 | -2.000E-04 | -1.180E-04 |
| $a_{V1}$ (mm$^{-1}$) | 1.730E-03 | 1.880E-03 | 8.780E-03 |
| $a_{V2}$ (mm$^{-1}$) | -5.000E-07 | 9.000E-07 | 8.000E-06 |
| $a_{L1}$ | 5.560E-02 | 2.027E-01 | 9.693E-01 |
| $a_{L2}$ | 2.880E-02 | 2.610E-02 | 1.000E-02 |

*Table 3: Model coefficients and constants for the atmosphere.*

The total transmittance through the atmosphere along the line of sight, $\tau$ is given by

$$\tau = \exp(-sec(\theta)(A_O + A_V + A_L)), \qquad (5)$$

where $\theta$ is the incidence angle, $A_O$, $A_V$ and $A_L$ denote the vertically integrated adsorption components to oxygen, water vapour and liquid water, respectively. The approximations for $A_O$, $A_V$ and $A_L$ are given as

$$A_O = a_{O1} + a_{O2}(T_D - 270) \qquad (6a)$$

$$A_V = a_{V1}V + a_{V2}V^2 \qquad (6b)$$

$$A_L = a_{L1}[1 - a_{L2}(T_L - 283)]L, \qquad (6c)$$

(see Eq. 28-33 in Wentz and Meissner, 2000) where $L$ is in millimetres. $T_L$ is approximated by $(T_S + 273)/2$, which is the mean temperature of the cloud. The $a_O$ , $a_V$ and $a_L$ coefficients are given in Table 3 for all channels used for calculating sea-ice concentration.

The dielectric constant of sea water is a key component of the sea surface model. The parameter is a complex number that depends on frequency $v$, sea surface temperature $T_S$ and water salinity $s$. The dielectric constant is given as (see Eq. 35 in Wentz and Meissner, 2000)

$$\varepsilon = \varepsilon_R + \frac{\varepsilon_S - \varepsilon_R}{1 + [j\lambda_R/\lambda]^{1-\eta}} - \frac{2j\sigma\lambda}{C}, \tag{7}$$

where $j = \sqrt{-1}$, $\lambda = c/(v \times 10^9)$ in cm and $v$ is frequency. $\varepsilon_R$ is the dielectric constant at infinite frequency, $\varepsilon_S$ is the static dielectric constant, and $\lambda_R$ (cm) is the relaxation wavelength. The spread factor $\eta$ is an empirical parameter. The last term accounts for the conductivity of salt water, where $\sigma$ (sec$^{-1}$) is the ionic conductivity and $c$ is the speed of light ($3\times10^8$ m/s). It is generally assumed that $\eta$ and $\varepsilon_R$ are independent of temperature. The least squares fit yields $\eta = 0.012$ and $\varepsilon_R = 4.44$ (Wentz and Meissner, 2000).

Given the salinity $s = 35$ (‰), the conductivity of sea water is given by

$$\sigma = 3.39\,10^9 C^{0.892} \exp(-\Delta_t \zeta) \tag{8}$$

$$C = 0.5536\, s \tag{9a}$$

$$\Delta_t = 25 - t_s \tag{9b}$$

$$\zeta = 2.03\,10^{-2} + 1.27\,10^{-4}\Delta_t + 2.46\,10^{-6}\Delta_t^2 - C(3.34\,10^{-5} - 4.6\,10^{-7}\Delta_t + 4.6\,10^{-8}\Delta_t^2), \tag{9c}$$

where $C$ is chlorinity in percent and $t_S = T_S - 273.15$ in Celsius units.

The effect of salinity on $\varepsilon_S$ and $\lambda_R$ are modelled as (see Eq. 43-44 in Wentz and Meissner, 2000):

$$\lambda_R = 3.30 \exp(-0.0346\, t_S + 0.00017\, t_S^2) - 6.54\times10^{-3}(1 - 3.06\times10^{-2} t_S + 2.0\times10^{-4} t_S^2)s \tag{10}$$

$$\varepsilon_S = 87.9 \exp(-0.004585\, t_S) \exp(-3.45\text{E-}3\, s + 4.69\times10^{-6} s^2 + 1.36\times10^{-5} s \cdot t_S). \tag{11}$$

Once the dielectric constant $\varepsilon$ is known, the $V$ (vertical polarisation) and $H$ (horizontal polarisation) reflectivity coefficients $\rho_V$ and $\rho_h$ for a specular (i.e. perfectly flat) sea surface are calculated from the Fresnel Equations:

$$\rho_v = \frac{\varepsilon\cos\theta - \sqrt{\varepsilon - \sin^2\theta}}{\varepsilon\cos\theta + \sqrt{\varepsilon - \sin^2\theta}} \tag{12a}$$

$$\rho_h = \frac{\cos\theta - \sqrt{\varepsilon - \sin^2\theta}}{\cos\theta + \sqrt{\varepsilon - \sin^2\theta}}, \tag{12b}$$

where $\theta$ is the incidence angle. The specular reflectivity $R_0$ is then given as (see Eq. 46 in Wentz and Meissner, 2000):

$$R_{0v} = |\rho_v|^2 + \Delta R_{0v} \quad (13a)$$

$$R_{0h} = |\rho_h|^2 \quad (13b)$$

$$\Delta R_{0v} = 4.887 \times 10^{-8} - 6.108 \times 10^{-8} (T_S - 273)^3 . \quad (13c)$$

Wentz and Meissner (2000) proposed to add a correction term, as defined in Eq. 13c, to the V polarization reflectivity. The correction can lead to changes in the brightness temperature range from about +0.14 K in cold water to about -0.36 K in warm water.

The microwave emission from the ocean depends on surface roughness. A calm sea surface is characterized by a highly polarized emission. When the surface becomes rough, the emission increases and becomes less polarized, except at $\theta > 55°$ for which the vertically polarized emission decreases.

The rough sea surface reflectivity $R$ is given as

$$R = (1 - E_W) R_{geo} , \quad (14)$$

where the reflectivity $R_{geo}$ is given by the standard geometric optics model as (see Eq. 57 in Wentz and Meissner, 2000):

$$R_{\text{geo}} = R_0 - [r_0 + r_1(\theta - 53) + r_2(T_S - 288) + r_3(\theta - 53)(T_S - 288)] W . \quad (15)$$

The first term $R_0$ is the specular reflectivity given by Eq. 13 and the second term is the wind-induced component of the sea surface reflectivity. The *r* coefficients are given in Table 4 for all channels used for calculating sea-ice concentrations.

The $E_W$ term that accounts for both foam and diffraction effects is found to be a monotonic function of wind speed $W$ as (see Eq. 60 in Wentz and Meissner, 2000):

$$E_W = m_1 W \qquad W < W_1 \quad (16a)$$

$$E_W = m_1 W + 0.5 (m_2 - m_1)(W - W_1) 2/(W_2 - W_1) \qquad W_1 \leqslant W \leqslant W_2 \quad (16b)$$

$$E_W = m_2 W - 0.5 (m_2 - m_1)(W_2 + W_1) \qquad W > W_2 , \quad (16c)$$

where $W_1 = 3$ m/s and $W_2 = 12$ m/s for the V polarisation, and $W_1 = 7$ m/s and $W_2 = 12$ m/s for the H polarisation, respectively. The *m* coefficients are given in Table 4 for all used for the sea-ice concentration calculations.

| Coeff.\Freq. GHz | 19 V | 37 V | 37 H | 89 V | 89 H |
|---|---|---|---|---|---|
| $r_0$ (s/m) | -0.49E-3 | -1.01E-3 | 1.91E-3 | -1.53E-3 | 2.02E-3 |
| $r_1$ (s/m-deg) | -0.53E-4 | -1.05E-4 | 1.12E-4 | -1.16E-4 | 1.30E-4 |
| $r_2$ (s/m-K) | 0.48E-5 | 1.27E-5 | -0.36E-5 | 1.15E-5 | 0.00E-5 |
| $r_3$ (s/m-deg-K) | 0.31E-6 | 0.45E-6 | -0.36E-6 | -0.09E-6 | -0.46E-6 |
| $m_1$ (s/m) | 0.00140 | 0.00257 | 0.00329 | 0.00260 | 0.00330 |
| $m_2$ (s/m) | 0.00736 | 0.00701 | 0.00660 | 0.00700 | 0.00660 |
| $E_{ice}$ | 0.95 | 0.93 | 0.88 | 0.8 | 0.75 |
| $T_{mix}$ | 0.75 | 0.95 | 0.70 | 0.97 | 0.97 |

*Table 4: Model coefficients and constants for the sea surface with polarization.*

Atmospheric radiation scattered by the sea surface $T_{B\Omega}$ can be approximated as (see Eq. 61 in Wentz and Meissner, 2000):

$$T_{B\Omega}=[(1+\Omega)(1-\tau)(T_D-T_C)+T_C]R, \quad (17)$$

where $R$ is the sea surface reflectivity given by Eq. 14, $T_D$ is the down-welling brightness temperature given by Eq. 2 and $T_C$ is a constant (2.7 K) representing the cosmic background radiation temperature. $\Omega$ is the fit parameter given for V polarization and H polarization, respectively:

$$\Omega_v=[2.5+0.018(37-v)](\sigma^2-70.0\times\sigma^6)\tau^{3.4} \quad (18a)$$
$$\Omega_h=[6.2-0.001(37-v)^2](\sigma^2-70.0\times\sigma^6)\tau^2, \quad (18b)$$

where $v$ is frequency (GHz) and $\sigma^2$ is the sea surface slope variance,

$$\sigma^2=5.22\times10^{-3}W \qquad v\geq37\,\text{GHz} \quad (18c)$$
$$\sigma^2=5.22\times10^{-3}[1-0.00748(37-v)^{1.3}]W \qquad v<37\,\text{GHz}. \quad (18d)$$

The term $\sigma^2 - 70.0\times\sigma^6$ has a maximum at $\sigma^2 = 0.069$. For $\sigma^2 > 0.069$, the term is held at its maximum value of 0.046. $\Omega_h$ has a quadratic dependence on frequency with a maximum value at $v = 37$ GHz. For $v > 37$ GHz, both $\Omega_v$ and $\Omega_h$ are held constant at their maximum values. The approximation for $\Omega_v$ and $\Omega_h$, given by Equations 18a and 18b are valid for the range of incidence angles from 52° to 56°.

The sea surface emissivity, $E$, is given by Kirchhoff's law to be

$$E=1-R. \quad (19)$$

Finally, the simplified radiative transfer Equation for the brightness temperature from the atmosphere over open water (i.e. Eq. 1) and sea-ice covered surfaces:

$$T_b=T_{BU}+\tau[(1-C_{ice})ETs+(1-C_{ice})(1-E)(T_{B\Omega}+\tau T_C)+C_{ice}E_{ice}T_{ice}+C_{ice}(1-E_{ice})(T_{BD}+\tau_{TC})], \quad (20)$$

where $E_{ice}$ is the sea-ice emissivity and the ice effective temperature $T_{ice}$ has a linear relationship between sea surface and freezing point of 271.35 K.

$$T_{ice}=T_{mix}T_s+271.35(1-T_{mix}) \quad (21)$$

if $T_{ice} \leq 0$, then $T_{ice} = 0$; if $T_{ice} \geq 271.35$ K, then $T_{ice} = 271.35$ K. Both $E_{ice}$ and $T_{mix}$ are channel dependent, given in Table 4 for all channels used to compute sea-ice concentration. $C_{ice}$ is the sea-ice concentration, a fraction from 0 to 1 (indicating from no sea-ice to 100 % covered by sea-ice).

## 5. Dynamic tie-points

The tie-points for sea-ice and open water are the set of brightness temperature values that correspond to sea-ice concentrations of 100 % and 0 %, respectively. They are used in the sea-ice concentration algorithms as a reference. The tie-points are derived by selecting $T_b$s from regions of known 100

% open water and 100 % sea-ice. Usually these tie-points are static in time and space, but they can be adjusted to follow the seasonally changing signatures of sea-ice and open water. Static tie-points are prone to be affected by sensor drift, inter sensor calibration differences and climatic trends in surface and atmospheric emission. The data must therefore be carefully calibrated before computing the sea-ice concentrations. Here, we use dynamic tie-points, a method that minimizes these unwanted effects, with or without prior calibration.

During winter, in the consolidated pack sea-ice well within the sea-ice edge, the sea-ice concentration is very near 100 % (Andersen et al., 2007). This has been established using high resolution SAR data, ship observations and by comparing the estimates from different sea-ice concentration algorithms. The apparent fluctuations in the derived sea-ice concentration in the near 100 % sea-ice regime are primarily attributed to snow/ice surface emissivity variability around the tie-point signature and only secondarily to actual sea-ice concentration fluctuations. In the marginal sea-ice zone the atmospheric emission may be significant. The fluctuations due to atmospheric and surface emission are systematic. In fact, different algorithms with different sensitivity to atmospheric and surface emission compute very different trends in sea-ice area on seasonal and decadal time scales (Andersen et al., 2007). This means that not only the sea-ice area have a climatic trend, but the atmospheric and surface constituents affecting the microwave emission are also changing. For example, different wind patterns, water vapour and liquid water concentrations in the atmosphere, snow depth, fraction of perennial sea-ice etc. In an attempt to compensate for the influence of these unwanted trends the tie-points are derived dynamically using a mean of the last 30 days of swath data. It is assumed that sea-ice concentrations from the NT algorithm above 95 % are in fact near 100 % sea-ice, and that the mean value of these data points can be used to derive the sea-ice tie-point. The NT sea-ice concentration is the initial guess, before the iteration, and the OSI SAF sea-ice concentration does not depend on the NT sea-ice concentration. The analysis of SAR data in Andersen et al. (2007) from the central Arctic showed that, during winter, there is more than 99 % sea-ice cover. During strong ice drift divergence and during the summer there may be situations where this is not the case. However, during one month of tie-point data collection we are sure to have captured the situations with near 100 % sea-ice cover. The standard deviation of the tie-point is included in the total sea-ice concentration error estimate which is the justification for this assumption.

Regions of open water are selected near the sea-ice edge using the monthly NSIDC maximum sea-ice extent climatology plus additional 100 km. There is no attempt to compensate explicitly for sensor drift or inter-sensor calibration differences between the seven different sensors used in the analysis. The dynamic tie-point method is in principle compensating for these problems in a consistent manner.

Dynamic tie-point algorithm summary:

1. For each swath grid point the NT sea-ice concentration (static tie-points, Comiso et al. 1997) is added.
2. The atmospheric correction is applied based on the NT sea-ice concentration and the NWP data.
3. The dynamic tie-points are computed using the swath data for one day i.e. the number of data points for the sea-ice and the water tie-points, the coordinates for the sea-ice line and for the water point. Dynamic tie-points are computed separately for the Bristol algorithm, the Bootstrap algorithm and the algorithm 89 GHz linear. The two sets for the first two algorithms are used by

the OSI SAF hybrid algorithm, and the sets for the last two algorithms are used by the TUD hybrid algorithm (see the next section).

4. The daily tie-point coordinates are combined into a 30 day running mean tie-point which is used in the further processing.

# 6. The sea-ice concentration algorithms

This section describes the two algorithms that are used to compute the sea-ice concentrations: the OSI SAF hybrid and the TUD. The OSI SAF hybrid algorithm is applied to generate sea-ice concentration to both the AMSR-2 and SSMIS product; it uses the 19 H, 19 V and 37 H channels. The TUD algorithm is only applied to genearate the AMSR-2 product and not the SSMIS. It uses the 19 V, 37 V, 89 V and 89 H channels, and is capable of higher resolution than the OSI SAF hybrid algorithm, but is more susceptible to noise due to water vapour.

## 6.1. The OSI SAF hybrid algorithm

A total of 30 algorithms retrieving Arctic sea-ice concentration from satellite passive microwave data are described and compared in detail in the SICCI ATBD (ESA SICCI project consortium, 2013). The analysis of atmospheric sensitivity in Andersen et al. (2006B) showed that the Bootstrap frequency mode algorithm (Comiso, 1986) had the lowest sensitivity to atmospheric noise over open water. Furthermore, the comparison to high resolution SAR imagery in Andersen et al. (2007) revealed that among the algorithms using the low frequency channels (19 and 37 GHz), the Bristol algorithm (Smith, 1996) had the lowest sensitivity to sea-ice surface emissivity variability. In addition, this algorithm had a low sensitivity to atmospheric emission in particular at high ice concentrations. Consequently, a hybrid algorithm has been established as a linear combination of two of the tested algorithms, the Bristol algorithm and the Bootstrap frequency mode algorithm. To ensure an optimum performance over both marginal and consolidated sea-ice, and to retain the virtues of each algorithm, the Bristol algorithm is given little weight at low concentrations, while the opposite is the case over high sea-ice concentrations.

The Bootstrap algorithm (Comiso, 1986) is based on the observation of linear clustering of sea-ice $T_b$s in scatter plots of $T_{37V}$ vs $T_{19V}$ whereas open water $T_b$s cluster around a single point. It assumes only two surface types: sea-ice and open water, taking into account the variability of both to optimize the detection of small sea-ice concentrations. The linear relationship yields the following simple formulation for the total sea-ice concentration, $C_{\text{bootstrap}}$:

$$C_{\text{bootstrap}} = \left(T_b - T_b^W\right) / \left(T_b^I + T_b^W\right) 100, \tag{22}$$

where $T_b$ is the measured brightness temperature, $T_b^W$ and $Tb^I$ are the open water tie-point and the sea-ice tie-point, respectively, both in the unit of temperature.

The Bristol algorithm (Smith, 1996) is conceptually similar to the Bootstrap algorithm. In a three-dimensional scatter plot spanned by $T_{19V}$, $T_{37V}$ and $T_{37H}$ the sea-ice $T_b$'s tend to lie in a plane. The only difference to the Bootstrap algorithm is that instead of viewing the data in the $T_{19V}$, $T_{37V}$ space, the Bristol algorithm views the data perpendicular to the plane in which the data lies, i.e. in a transformed coordinate system:

$$\text{Bristol}_x = T_{37V} + 1.045\,T_{37H} + 0.525\,T_{19H}, \quad (23a)$$

$$\text{Bristol}_y = 0.9164\,T_{19V} - T_{37V} + 0.4965\,T_{37H}. \quad (23a)$$

The remaining analysis is identical to the Bootstrap algorithm.

The Bootstrap algorithm is used over open water and the Bristol algorithm is used over sea-ice. At concentrations of up to 40 % the sea-ice concentration is an average weighted linearly between the two algorithms, as shown in Eq. 24. This hybrid algorithm is the OSI SAF sea-ice concentration algorithm.

$$\begin{aligned} C_{tot} &= (1 - \text{weight})\,C_{\text{bristol}} + \text{weight}\,C_{\text{bootstrap}}, \\ \text{weight} &= (|\text{threshold} - C_{\text{bootstrap}}| + \text{threshold} - C_{\text{bootstrap}})/(2\,\text{threshold}), \end{aligned} \quad (24)$$

where threshold is 40 %.

### 6.2. The TUD hybrid algorithm

The TUD sea-ice concentration algorithm is using the part of the Bootstrap algorithm which is normally used over open water (Comiso, 1986; Comiso et al., 1997) together with the scaled h and v polarisation difference of the near 90 GHz channels (Pedersen, 1998). The Bootstrap algorithm in frequency mode has relatively coarse resolution but it is almost independent of different weather conditions.

The TUD hybrid algorithm is a combination of the coarse resolution sea-ice concentration $C_f$, determined by the Bootstrap algorithm in frequency mode, and the high resolution sea-ice concentration $C_{89}$, determined by the algorithm 89 GHz linear with dynamic tie-points. Both are calculated by Eq. 22, with different input of brightness temperature, $T_{19V}$ and $T_{37V}$ for $C_f$ and $T_{89V}$ and $T_{89H}$ for $C_{89}$.

A comparison between $C_f$ and $C_{89}$ shows that there is larger scatter, in particular at the low sea-ice concentrations derived from 89 GHz compared to the lower frequency channels (Pedersen, 1998). In order to reduce the noise in $C_{89}$, the TUD algorithm is adjusted as:

If $C_{89} > 0$ and $C_f > 10$, the total sea-ice concentration, $C$

$$C = \sqrt{(C_f\,C_{89})}, \quad (25)$$

otherwise, the total sea-ice concentration, $C$ *is*

$$C = C_f. \quad (26)$$

## 7. Sea-ice concentration uncertainties

Uncertainty estimates are needed when the sea-ice concentration data are compared to other data sets or when the sea-ice concentrations are assimilated into numerical models. The mean accuracy of some of the more common algorithms, used to compute sea-ice concentration from SSM/I data, such as the NT and Bootstrap algorithms are reported to be 1-6 % in winter (Andersen et al., 2006A). This is also achieved with the OSISAF algorithm (Ivanova et al., 2015).

The polar atmosphere is generally transparent for microwave radiation in between the sounding channels called the atmospheric windows near 19, 37, 91, and 150 GHz. For typical polar atmospheric states the down-welling emission at the surface is about 5-15 K at 18 GHz, 20-40 K at 36 GHz, 30-100 K at 90 GHz. For comparison, the sea-ice surface emission is typically 150-260 K. When computing the sea-ice concentration using the atmospheric window channels, the atmospheric emission and scattering is an error source. The tie-points are typical sea-ice and water signatures representative on a hemispheric scale. Deviations from the typical surface emission signatures result in sea-ice concentration uncertainties. The AMSR-2 instrument has relatively large foot-prints on the ground, and the algorithms with the lowest sensitivity to both atmospheric and surface emissivity variability use $T_b$s at different frequencies with different foot-print size. Representing these large foot-prints on a finer, predefined grid results in a representativeness error. In addition there is the geo-location error, sensor noise, drift, and sea-ice variability over the sampling period.

We assume the total uncertainty as

$$\sigma_{tot}^2 = \sigma_{algo}^2 + \sigma_{smear}^2 , \tag{27}$$

where $\sigma_{\text{algo}}$ is the inherent uncertainty of the concentration algorithm and $\sigma_{smear}$ is the uncertainty due to the foot print mismatch to a grid where the sensor footprint covers more than one pixel.

## 7.1. Algorithm and tie-point uncertainties

Both the water surface and sea-ice surface emissivity variabilities result in sea-ice concentration uncertainties. Emission and scattering in the atmosphere also affects the $T_b$s and the computed sea-ice concentrations. Different algorithms have different sensitivities to these surface and atmospheric parameters (Andersen et al., 2006B). Further, both the atmospheric and surface parameters affecting the sea-ice concentration estimates have climatic trends (Andersen et al., 2007). To minimize the uncertainties due to these two parameters, the $T_b$s are corrected using NWP data for atmospheric humidity and open water roughness in this reanalysis. The dynamic tie-points minimizes uncertainty due to the climatic trends in the atmosphere and on the sea-ice surface on a hemispheric scale while regional trends may still exist.

The errors are computed using the hemispheric standard deviation of the measurements over open water and over near 100 % sea-ice respectively. The sea-ice concentration algorithm provides sea-ice concentrations which are greater than 100 % and less than 0 %. These non-physical concentrations are truncated in the processing. Therefore we write the sea-ice concentration, $\text{ic}$:

$$\text{ic} = (1 - \alpha(\text{ic}))\,\text{water} + \alpha(\text{ic})\,\text{ice} , \tag{28}$$

where $\text{ic}$ is the sea-ice concentration calculated by the algorithm and $\alpha$ is the truncated sea-ice concentration as a function of $\text{ic}$

$$\alpha(ic) = \prod(\text{ic})\,ic + H(\text{ic} - 1) , \tag{29}$$

where $\prod(x)$ is the Boxcar function and $H(x)$ the Heaviside step function. The functional dependency between $\alpha$ and $\text{ic}$ is described by

$$\alpha = 0 \qquad \mathrm{ic} \leqslant 0$$
$$\alpha = \mathrm{ic} \qquad 0 < \mathrm{ic} < 1$$
$$\alpha = 1 \qquad \mathrm{ic} \geqslant 1.$$

Using Eq. 29 and assuming the uncertainty for the sea-ice and water part is independent, leads to a total algorithm uncertainty as

$$\sigma_{\mathrm{algo}}(\alpha(\mathrm{ic})) = \sqrt{(1-\alpha(\mathrm{ic}))^2 \sigma^2_{\mathrm{water}} + \alpha^2(\mathrm{ic})\sigma^2_{\mathrm{ice}}}, \tag{30}$$

where

$$\sigma_{\mathrm{water}} = \sigma(\mathrm{IC}(P_{\mathrm{openwater}})) \tag{31}$$

and open water is determined by a monthly varying ocean mask, $\mathrm{IC}$ is the functional mapping of the sea-ice concentration algorithm and $P_C$ denotes the set of swath pixels for all swaths (used for calculating the daily product) selected on the condition $C$. The condition $C$ is either sea-ice or water.

The standard deviation of the sea-ice concentrations is given by

$$\sigma_{ice} = \sigma(\mathrm{IC}(P_{\mathrm{ocean,NT}>0.95})), \tag{32}$$

where the NT algorithm finds sea-ice concentrations greater than 0.95.

## 7.2. Representativeness error

Foot-print sizes for the channels used for sea-ice concentration mapping range from about 56 km for the 19 GHz channels on SSMIS, to about 36 km for the 37 GHz channels on the same satellite (Table 1 and 2). AMSR-2 resolutions are about 18 km at 19 GHz, 10 km at 37 GHz and 4 km on 89 GHz. Foot-prints of these uneven size are combined in the sea-ice concentration algorithms when computing the sea-ice concentration and this results in a representativeness uncertainty also called a foot-print mismatch uncertainty. This foot-print mismatch uncertainty is accepted because it gives higher spatial resolution sea-ice concentrations than if the higher frequency channels were re-sampled to the coarser resolution channels before computing the sea-ice concentration and channels at different frequencies are combined to reduce sea-ice concentration noise.

The foot-print mismatch uncertainty is computed using a microwave radiometer imaging simulator and quantified as coefficients in the uncertainty algorithm. Each data point in the file is a representation of the sea-ice concentration within the foot-print and weighted with the foot-prints. The SSMIS OSISAF sea-ice concentration has a foot-print size of 35×57 km, the AMSR-2 OSISAF sea-ice concentration has a foot-print size of 11×17 km, the AMSR-2 TUD sea-ice concentration has a foot-print size of 7×11 km.

## 7.3. Geolocation error

Geolocation error occur due to uncertainties in the orientation of the satellite. For both SSMIS and AMSR2, the RMSE geolocation error is approximately 5 km for the 6.9 GHz channel (~10 % of the beam FWHM footprint dimensions), reducing to 1 km for the 89 GHz channel (~20 % of the beam FWHM footprint dimensions).

## 8. Climatology Mask

The Level-3 product uses gridded monthly maximum climatology masks, to remove spurious ice from the areas where it has been historically ice free. Polygon masks are used for the Level-2 product, as gridded masks are not well suited for use with Level-2 products. The climatology mask is derived from the monthly sea ice extent dataset (Fetterer et al. Sea Ice Index), covering from 1978-11 to 2019-10, which is available via FTP from:

ftp://sidads.colorado.edu/pub/DATASETS/NOAA/G02135/north/monthly

ftp://sidads.colorado.edu/pub/DATASETS/NOAA/G02135/south/monthly

for the Northern and Southern hemispheres respectively. For a given month, the climatology mask covering both hemispheres is created as follows: for each hemisphere, the sea ice extent polygons for all years for the month are merged to obtain the maximum extent polygon; then these Northern and Southern Hemisphere polygons are then reprojected to an Azimuthal Equidistant projection; next, the polygon for the Northern and Southern Hemispheres are reprojected to an Azimuthal Equidistant projection before being combined into a single object (It is necessary that the mask covers both hemispheres because the swaths covers both.) A 300 km buffer is applied to the mask. Finally, each of the twelve masks (one for each month) are written to shape files. Figure 2 shows the climatology mask for April.

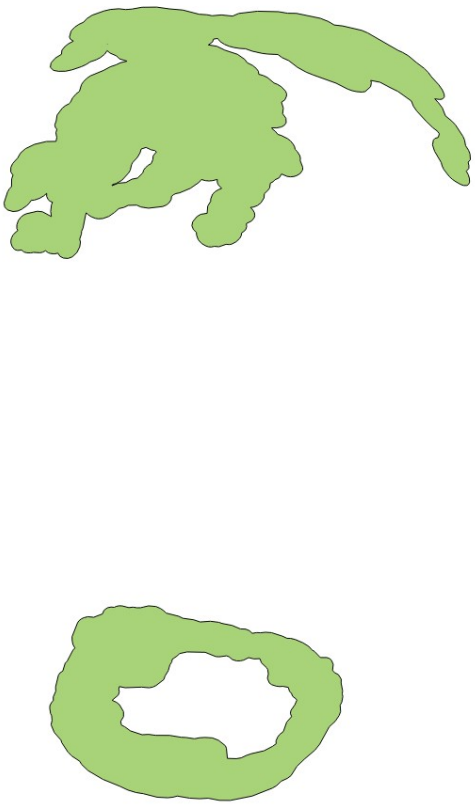

*Figure 2: Maximum climatology mask for sea ice extent covering the Northern and Southern Hemispheres in the Azimuthal Equidistant projection.*

## 9. Land Mask

The Global Self-consistent, Hierarchical, High-resolution Geography Database (GSHHG), displayed in Figure 3, is a polygon coastline (Wessel, P. et al.) used to mask observations over land. The “intermediate” land/lake mask is used. Lakes with an area of 15,000 km2 are not masked.

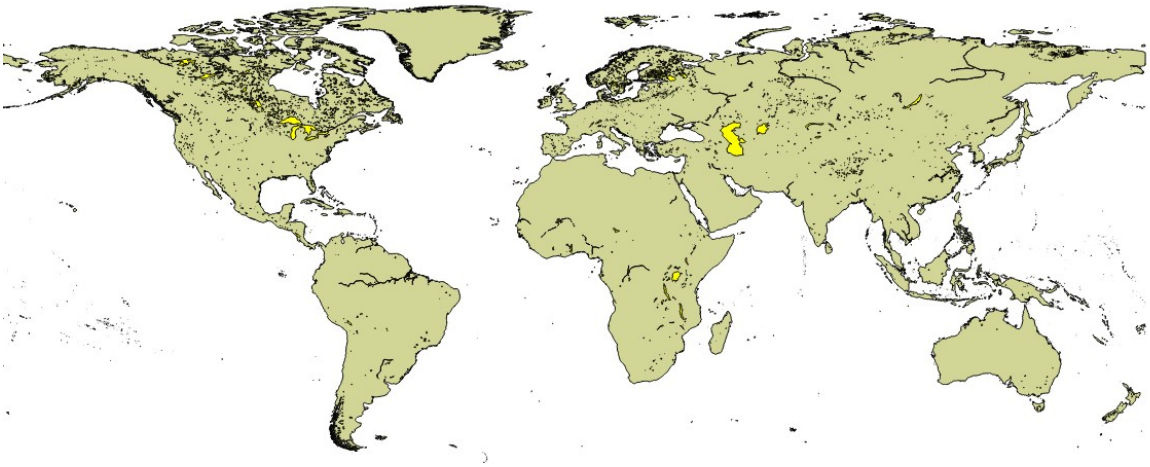

*Figure 3: GSHHG coastline and lake mask*

## 10. References


Andersen, S., L. Toudal Pedersen, G. Heygster, R. Tonboe, and L Kaleschke, Intercomparison of passive microwave sea ice concentration retrievals over the high concentration Arctic sea ice. *Journal of Geophysical Research* 112, C08004, doi10.1029/2006JC003543, 2007.

Andersen, S., R. T. Tonboe and L. Kaleschke. Satellite thermal microwave sea ice concentration algorithm comparison. *Arctic Sea Ice Thickness: Past, Present and Future*, edited by Wadhams and Amanatidis. Climate Change and Natural Hazards Series 10, EUR 22416, 2006A.

Andersen, S., R. Tonboe, S. Kern, and H. Schyberg. Improved retrieval of sea ice total concentration from spaceborne passive microwave observations using Numerical Weather Prediction model fields: An intercomparison of nine algorithms. *Remote Sensing of Environment104, 374-392*, 2006B.

Comiso J.C, D.J. Cavalieri, C.L. Parkinson, and P. Gloersen. Passive microwave algorithms for sea ice concentration: A comparison of two techniques. *Remote Sensing of Environment* 60, 357-384, 1997.

Comiso J.C. Characteristics of arctic winter sea ice from satellite multispectral microwave observations. *Journal of Geophysical Research* 91(C1), 975-994, 1986.

ESA SICCI project consortium. D2.6: Algorithm Theoretical Basis Document (ATBDv1), ESA Sea Ice Climate Initiative Phase 1 Report SICCI-ATBDv1-04-13, version 1.1, 2013.

Fetterer, F., K. Knowles, W. N. Meier, M. Savoie, and A. K. Windnagel. 2017, updated daily. *Sea Ice Index, Version 3*. [Monthly sea ice extent]. Boulder, Colorado USA. NSIDC: National Snow and Ice Data Center. doi: https://doi.org/10.7265/N5K072F8. [2019-11-01].

Imaoka, K., M. Kachi, M. Kasahara, N. Ito, K. Nakagawa and T. Oki. Instrument performance and calibration of AMSR-E and AMSR2. International Archives of the Photogrammetry, Remote Sensing and Spatial Information Science, 38(8), 13-18, 2010.

Ivanova, N., L. T. Pedersen, R. T. Tonboe, S. Kern, G. Heygster, T. Lavergne, A. Sørensen, R. Saldo,G. Dybkjær, L. Brucker, and M. Shokr. Inter-comparison and evaluation of sea ice algorithms: towards further identification of challenges and optimal approach using passive microwave observations. The Cryosphere, 9, 1797–1817, 2015.

Markus T, Cavalieri D. The AMSR-E NT2 Sea Ice Concentration Algorithm: its Basis and Implementation. *Journal of The Remote Sensing Society of Japan*. 2009; 29 (1):216-225.

Pedersen, L.T. Chapter 6.2 in Sandven et al. IMSI report no. 8. Development of new satellite ice data products (Chapter 6.2). Bergen, Norway: NERSC Technical Report no.145, Nansen Environmental and Remote Sensing Center, Bergen, Norway, 1998.

Smith, D. M. Extraction of winter total sea ice concentration in the Greenland and Barents Seas from SSM/I data. *International Journal of Remote Sensing 17*(13), 2625-2646, 1996.

Wessel, P., and W. H. F. Smith (1996), A global, self-consistent, hierarchical, high-resolution shoreline database, J. Geophys. Res., 101(B4), 8741–8743, doi:10.1029/96JB00104.

Wentz, F. J. A well-calibrated ocean algorithm for SSM/I. *Journal of Geophysical Research* 102(C4), 8703-8718, 1997.

Wentz, F. J., Meissner, T. (2000). AMSR ocean algorithm version 2. RSS Tech. Proposal 121599A-1, Remote Sensing Systems, Santa Rosa, California.